

# Tomographic traveltimes inversion using natural pixels

R. J. Michelena\* and J. M. Harris\*

### ABSTRACT

Traditionally in the problem of tomographic traveltimes inversion, the model is divided into a number of rectangular cells of constant slowness. Inversion consists of finding these constant values using the measured traveltimes. The inversion process can demand a large computational effort if a high-resolution result is desired.

We show how to use a different kind of parameterization of the model based on beam propagation paths. This parameterization is obtained within the framework of reconstruction in Hilbert spaces by minimizing the error between the true model and the estimated model. The traveltimes are interpreted as the projections of the slowness along the beampaths. Although the actual beampaths are described by complicated spatial functions, we simplify the computations by approximating these functions with functions of constant width and height, i.e., "fat" rays, which collectively form a basis set of natural pixels.

With a simple numerical example we demonstrate that the main advantage of this parameterization, compared with the traditional decomposition of the model in rectangular pixels, is that 2-D reconstructed images of similar quality can be obtained with considerably less computational effort. This result suggests that the natural pixels can provide considerable computational advantage for 3-D problems.

### INTRODUCTION

The process of reconstructing an image using line integrals through it is called tomography. In traveltimes tomography the image to be reconstructed is the slowness model  $S(\mathbf{r})$ . The reconstructed model  $\tilde{S}(\mathbf{r})$  is usually represented as a linear combination of functions  $\beta_n(\mathbf{r})$  in the form

$$\tilde{S}(\mathbf{r}) = \sum_{n=1}^M a_n \beta_n(\mathbf{r}). \tag{1}$$

The problem consists of determining the unknown coefficients  $a_n$  from the measured traveltimes. Once these coefficients have been calculated, the computation of the sum (1) is straightforward.

The representation (1) has two important degrees of freedom that influence decisively the kind of results obtained. These are the number ( $M$ ) and kind of functions  $\beta_n(\mathbf{r})$  to be used. The most common choice for the functions  $\beta_n(\mathbf{r})$  is orthogonal cells (square or cubic pixels), and in that case the coefficients  $a_n$  represent the slowness within each cell (McMechan, 1983; Ivansson, 1985). Although this is the most popular basis function for estimating the slowness model, others have been suggested recently. Harlan (1989) defines the velocity function as a sum of smooth basis functions (Gaussians), and Van Trier (1988) defines the functions  $\beta_n(\mathbf{r})$  as cubic B-splines multiplied by functions that reproduce the expected structure of the model. The number of functions  $M$  is also arbitrary but is usually small to avoid having to solve a huge system of equations.

The kind and number of functions used for expanding the slowness model determine many of the general features of the final image. With the same data set it is possible to obtain different results just because different parameterizations have been used. However, the goal is to obtain a reconstructed model free from these artifacts of parameterization, which means the selection of the basis function is critical in the inversion process and thus should be considered more carefully, as described below.

There are no general criteria for deciding which representation is the best, although some may have clear advantages for solving specific problems. Our selection of the basis function will be based on minimization of the expression that estimates the norm of the null space of the problem

$$\left\| S(\mathbf{r}) - \sum_{n=1}^M a_n \beta_n(\mathbf{r}) \right\|, \tag{2}$$

Manuscript received by the Editor December 15, 1989; revised manuscript received September 11, 1990.

\*Department of Geophysics, Stanford University, Stanford, CA 94305.

© 1991 Society of Exploration Geophysicists. All rights reserved.

where  $S(\mathbf{r})$  is the true slowness model. Due to the nature of the measurements in travelt ime tomography (integral along beampaths), we show that the minimum of expression (2) can be reached when the functions  $\beta_n(\mathbf{r})$  describe the beampaths and when  $M$  equals the number of measurements available (because there is only one measurement per beam-path). The first part of the paper demonstrates this fact within the framework of reconstruction in Hilbert spaces. The remainder presents a comparison of the inversion of synthetic data using the traditional representation of the model in square pixels and the proposed representation in constant regions along the beampaths called natural pixels.

### RECONSTRUCTION IN HILBERT SPACES

A Hilbert space is a linear space on which an inner product is defined. For example, the inner product for the Hilbert space  $L^2$  of the Lebesgue square-integral functions of support  $\Omega$  is

$$\langle f(x), \beta(x) \rangle = \int_{\Omega} f(x)\beta(x) dx. \quad (3)$$

We can assume that the particular function  $f(x)$  that we want to estimate belongs to a Hilbert space  $H$ . Let's assume also that the information we have about  $f(x)$ , i.e., data, is a set of inner products of the function  $f(x)$  with a finite set of known functions  $\beta_m(x) \in H$

$$d_m = \langle f(x), \beta_m(x) \rangle \quad m = 1, \dots, N. \quad (4)$$

In this context, the data can be interpreted as the projections of the unknown function  $f(x)$  onto the "sampling" functions  $\beta_m(x)$ .

If  $F_1$  is a closed linear subspace of the Hilbert space  $H$ , then  $H = F_1 \oplus F_1^\perp$  (Berberian, 1976), where  $F_1^\perp$  is called the orthogonal complement of  $F_1$ . From the projection theorem (Stakgold, 1979), we can always decompose  $f(x)$  into  $f_1(x) + f_2(x)$  (Figure 1), where  $f_1(x) \in F_1$  and  $f_2(x) \in F_1^\perp$ ;  $f_1(x)$  is called the orthogonal projection of  $f(x)$  in  $F_1$ . If we assume that the functions  $\beta_n(x)$  form a basis of the space  $F_1$ , we can write

$$f(x) = \sum_{n=1}^N a_n \beta_n(x) + f_2(x). \quad (5)$$

The meaning of the function  $f_2(x)$  is explained by multiplying both sides of equation (5) by  $\beta_m(x)$  and integrating in  $\Omega$ :

$$d_m = \sum_{n=1}^N a_n \langle \beta_n(x), \beta_m(x) \rangle + \langle f_2(x), \beta_m(x) \rangle. \quad (6)$$

Since  $\langle f_2(x), \beta_m(x) \rangle = 0$ , we can say that  $f_2(x)$  contains the information about  $f(x)$  that does not affect the measurements made by the sampling functions  $\beta_m(x)$ . Finally, the estimate  $\bar{f}(x)$  of  $f(x)$  can then be written as

$$\bar{f}(x) = f_1(x) = \sum_{n=1}^N a_n \beta_n(x), \quad (7)$$

where the coefficients  $a_n$  are calculated from the forward equation for the data  $d_m$ ,

$$d_m = \sum_{n=1}^N a_n \langle \beta_n(x), \beta_m(x) \rangle \quad m = 1, \dots, N. \quad (8)$$

Note that the system of equations (8) is square. If all the sampling functions are independent, the problem is well conditioned and, therefore, the system (8) has a unique solution. A unique solution is expected because the orthogonal projection of  $f(x)$  in the space  $F_1$  expanded by the functions  $\beta_m(x)$  is unique (Figure 1). If any of the sampling functions can be expressed approximately as a linear combination of the others, the problem becomes ill conditioned since the rows (or columns) in the matrix of equation (8) are not independent any more.

### Minimum norm solution

This same result for  $\bar{f}(x)$  can be obtained through minimization of the norm  $\|f_2(x)\|$  with respect to the unknown coefficients  $a_n$  (Darling et al., 1983),

$$\min \|f_2(x)\|^2 = \min \left\| f(x) - \sum_{n=1}^N a_n \beta_n(x) \right\|^2. \quad (9)$$

For this reason, the estimate  $\bar{f}(x)$  is called the minimum norm estimate of the unknown function  $f(x)$ . This estimate

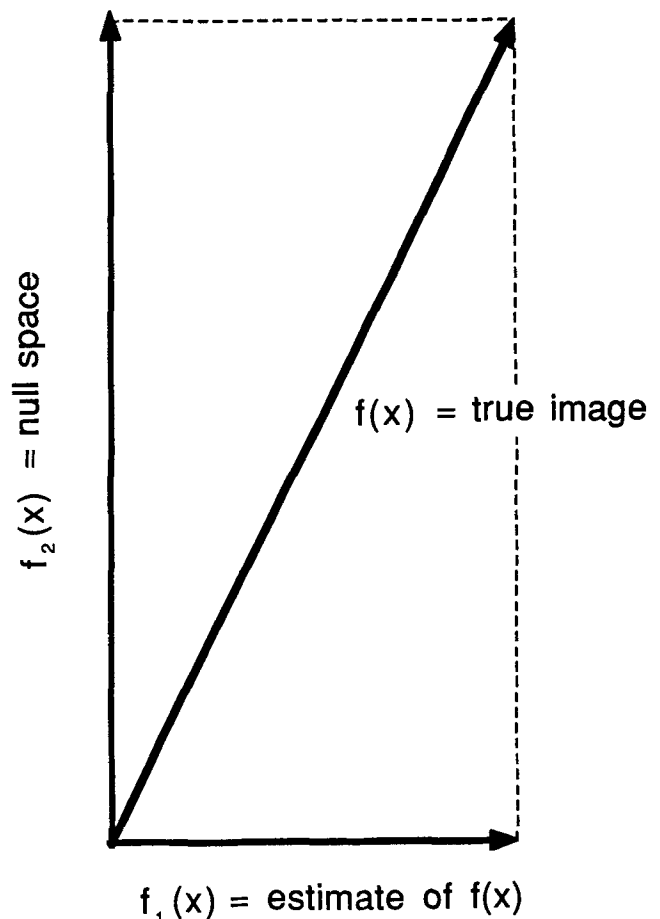


FIG. 1. Orthogonal projections of the true image.

$\tilde{f}(x)$  is unique and consistent with the data [equation (8)]; it is also strongly related to the way the modeled data are generated, because the unknown function  $f(x)$  is expressed as a linear combination of the sampling functions  $\beta_m(x)$  used to compute the forward modeling [equation (4)]. This means that each experiment will suggest “naturally” the reconstruction procedure which produces the minimum norm solution.

Examples of different sampling functions in different problems are the beampaths in the problem of traveltime tomography, complex exponentials when the measurements are the frequency components of  $f(x)$ , shifted versions of one function when the measurements represent the convolution of the unknown with a given filter, etc. When the measurements are the frequency components of  $f(x)$ , the minimum norm estimate is simply the Fourier series expansion of  $f(x)$  (Stakgold, 1979). In fact, equation (7) can be interpreted as a generalized Fourier series for basis sets not necessarily orthogonal.

If we expand  $\tilde{f}(x)$  in any other set of basis functions  $\{\alpha_n(x), n = 1, \dots, M\}$ , the norm of  $f_2(x)$  is

$$\|f_2(x)\| = \left\| f(x) - \sum_{n=1}^M c_n \alpha_n(x) \right\|. \quad (10)$$

Minimizing this expression with respect to the unknown coefficients  $c_n$ , we obtain

$$\langle f(x), \alpha_m(x) \rangle = \sum_{n=1}^M c_n \langle \alpha_n(x), \alpha_m(x) \rangle \quad m = 1, \dots, M. \quad (11)$$

Note that the independent term on the left-hand side in equations (11) is formed by the inner products of the selected basis function with the unknown function  $f(x)$ . Note also that the matrix elements are the inner products among the different elements of the selected basis. The independent term is equal to the measurements only if the basis set used for expanding  $\tilde{f}(x)$  ( $\{\alpha_n(x), n = 1, \dots, M\}$ ) is the same one used for generating the data, i.e.,  $\alpha_n = \beta_n$ . If any other basis set is used,  $\alpha_n \neq \beta_n$ , then the independent term must be computed from the measurements. Therefore, the choice  $\alpha_n = \beta_n$  is a convenient one among many other basis sets because the solution obtained is still minimum norm and the independent term in equation (11) directly represents the measurements. We will see later that in the problem of traveltime inversion the functions  $\beta_n(x, y)$  are the beampaths and then the minimum norm solution can be obtained easily from equation (7).

We illustrate these ideas with a simple example, which although not a geophysical case, can help explain why square orthogonal pixels are a convenient basis set when the measurements represent the average of the unknown over the same square regions. When the measurements have a different meaning, it might be computationally easier to get the minimum norm solution by using a different basis set. Consider a two-dimensional (2-D) object  $O(x, y)$  (a photograph, for example). The process of spatial discretization of the object can be interpreted as the convolution of  $O(x, y)$  and the sampling function  $R(x, y)$ , which describes the shape

of the pointer of the digitizer [for simplicity, the function  $R(x, y)$  is assumed to have unit area]

$$d(x, y) = O(x, y) * R(x, y), \quad (12)$$

where  $d(x, y)$  is the digitized image. This is equivalent to superimposing a square grid, for example, over the object and calculating the function  $d(x, y)$  from the volume of the object in the support of each pixel surrounding the grid point. This procedure can be expressed as

$$d_i = \int_{\Omega_i} O(x, y) R_i(x, y) dx dy, \quad (13)$$

where

$$R_i(x, y) = \begin{cases} 1 & \text{if } (x, y) \text{ is in the pixel } i \quad (i = 1, \dots, N) \\ 0 & \text{otherwise;} \end{cases} \quad (14)$$

$d_i, i = 1, \dots, N$  are the data points and  $\Omega_i$  is the support of the  $i$ th pixel.

Given the inner product (13), the minimum norm estimate of  $O(x, y)$  according to equation (7) is

$$\bar{O}(x, y) = \sum_{n=1}^N a_n R_n(x, y). \quad (15)$$

The coefficients  $a_n$  can be found from

$$d_m = \sum_{n=1}^N a_n \langle R_n(x, y), R_m(x, y) \rangle \quad m = 1, \dots, N. \quad (16)$$

According to the definition of  $R_i$ ,

$$\langle R_n(x, y), R_m(x, y) \rangle = \delta_{nm}. \quad (17)$$

Then,  $a_n = d_n$  and the estimate becomes

$$\bar{O}(x, y) = \sum_{n=1}^N d_n R_n(x, y). \quad (18)$$

As expected, the reconstructed object is formed with a superposition of  $N$  cells, each with constant height  $d_n$  and located where the measurements were taken. If we use any other basis set instead of  $R_i(x, y)$ , it is possible to get an estimate that does not reproduce the data, or requires more model parameters to get a better representation.

Fourier analysis is another example where the sampling functions  $\exp(ik_n x)$  are the same ones used to expand the estimate of the unknown. The result is also a minimum norm estimate.

The theory of reconstruction in Hilbert spaces generates consistent estimates of the unknown in the sense that the same basis set used to sample the function is used to expand it. The two previous examples (orthogonal sampling and Fourier reconstruction) confirm that in some situations this might be a convenient choice among many other possibilities. In the following sections we will exploit this idea of consistency in the problem of traveltime tomography where the data are generated in a very specific way (integrals along beampaths).

## TOMOGRAPHIC TRAVELTIME INVERSION

The traveltime along a ray  $\ell_m$  in a medium where the slowness is  $S(x, y)$  is traditionally given as

$$t_m = \int_{\ell_m} S(x, y) d\ell_m, \quad m = 1, \dots, N, \quad (19)$$

where  $d\ell_m$  is the incremental distance along the raypath  $\ell_m$ . In general, the raypath depends on the slowness distribution. For simplicity, we assume that the variations in the slowness are just a few percent. Then we can safely consider the raypaths as straight lines. (The general case will be discussed later.)

Although the expression (19) simplifies the mathematics considerably, it fails to convey the fact that the traveltimes between two points are affected by velocities in the region called the Fresnel zone, which is infinitely narrow only when the wavelength  $\lambda$  is infinitely small,  $\lambda \rightarrow 0$  (Nolet, 1987). To account for the finiteness of this effect, the traveltime between two points can be better described by the equation

$$t_m = \int_{\Omega} S(x, y) \phi_m(x, y) dx dy, \quad (20)$$

where  $\phi_m(x, y)$  is a 2-D function or "beam" of finite support centered along the raypath and  $\Omega$  is the support of  $S(x, y)$ . The functions  $\phi_m(x, y)$  can be interpreted as the wavepaths introduced by Woodward (1989).

With the forward modeling equation written in this way, the estimation of the slowness from the traveltimes can be seen as a reconstruction problem in a Hilbert space where the inner product is defined by equation (20). According to equation (7), the minimum norm estimate of the slowness  $S(x, y)$  is

$$\bar{S}(x, y) = \sum_{n=1}^N a_n \phi_n(x, y), \quad (21)$$

where  $N$  is the number of traveltimes.

We can transform equation (19) into a 2-D integral of the form of equation (20), if we describe the raypath with a 2-D delta function  $\delta_m(x, y)$ . However, the problem of reconstruction of the slowness from such an expression cannot be seen as a reconstruction problem in a Hilbert space because the inner product  $\langle \delta_i(x, y), \delta_i(x, y) \rangle$  is not defined.

From equation (8), the coefficients  $a_n$  can be calculated through the system of equations

$$t_m = \sum_{n=1}^N a_n \langle \phi_n(x, y), \phi_m(x, y) \rangle \quad m = 1, \dots, N, \quad (22)$$

where

$$\langle \phi_n(x, y), \phi_m(x, y) \rangle = \int_{\Omega} \phi_n(x, y) \phi_m(x, y) dx dy. \quad (23)$$

In contrast with the traditional reconstruction using square pixels as the basis functions [equation (18)], the reconstruction described above is based on a discretization of the model along the beampaths. In the previous example,

we showed that the square orthogonal pixels are a convenient discretization that lead to minimum norm estimators when the data are "point" orthogonal samples of the 2-D function we want to reconstruct. The discretization along the beampaths comes from the fact that they are the regions sampled with each measurement in traveltime tomography.

When the beampaths are used, the discretization of the model will depend in general on the particular data set to be inverted, because it will reflect the propagation of the energy in the medium. It does not have the advantage of other parameterizations that can reflect some prior knowledge about the model. In that sense, some flexibility is lost. The discretization along the beampaths is similar to the discretization of the model in square pixels in the way the prior information is handled, since both assume no prior information about the model. The difference is that when the problem is nonlinear and it is solved as a sequence of linearized steps, the discretization along the beampaths adapts progressively to the real model.

Note that although the solution of the system of equations (22) is unique, the null space of the problem has not been suppressed, only separated at the beginning of the formulation in the form of a space orthogonal to the beampaths [function  $f_2(x)$ , equation (5)]. The same situation occurs in discrete Fourier reconstruction, where for a given data set the estimate of the unknown is unique even though the null space (Fourier components above the Nyquist frequency) is not zero.

## Natural pixels

As a first approximation, we can describe the basis function  $\phi_i(x, y)$  as functions of width  $\lambda'$  and height  $1/\lambda'$

$$\phi_i(x, y) = \begin{cases} 1/\lambda' & \text{if } (x, y) \text{ is in the region of width} \\ & \lambda' \text{ centered along the raypath } i \\ 0 & \text{otherwise.} \end{cases} \quad (24)$$

Therefore, the matrix coefficients  $\langle \phi_n(x, y), \phi_m(x, y) \rangle$  are  $\langle \phi_n(x, y), \phi_m(x, y) \rangle \lambda'^2$

$$= \begin{cases} \text{area of the beampath} & \text{if } m = n \\ \text{area of the intersection} & \text{if } m \neq n. \end{cases} \quad (25)$$

A "natural pixel" for a single ray is shown in Figure 2. Even when the rays curve or when reflections are included, the natural pixels are strips centered on the raypath. The height of the strips may vary; for example, they can have a

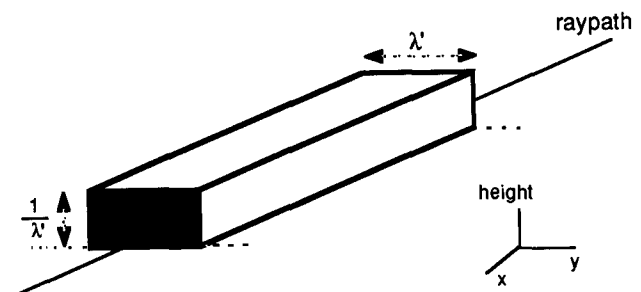


FIG. 2. Natural pixel as described in equation (24).

variable cross-section that gives more weight to the center than to the sides.

Buonocore et al. (1981) and Buonocore (1981), not working within the framework of reconstruction in Hilbert spaces, define an estimator identical to equation (21) and call it natural pixel decomposition of the two dimensional image, where the natural pixels are the functions  $\phi_m(x, y)$ . They study extensively the properties of such a reconstruction and the theoretical advantages of it compared with the traditional reconstruction using square pixels. They show that the matrix of coefficients  $\langle \phi_i(x, y), \phi_j(x, y) \rangle$  represents the measurement covariance matrix if there is no measurement noise. If the measurement noise is nonzero but uncorrelated, only the diagonal elements of the matrix are different from those of the measurement covariance matrix. According to Buonocore et al. (1981), square pixels errors are caused by the inaccurate estimation of the measurement covariance matrix. These errors can be eliminated only if the size of the pixels could be made infinitely small.

An example of a set of natural pixels is shown in Figure 3, for the case of a cross-borehole geometry in a medium of constant slowness. The details in the implementation of the inversion based on natural pixels are explained in the Appendix.

The number of cells in the square-pixel-based inversion is commonly determined by a tradeoff between the required resolution and cost of the inversion. With square pixels we are forced to establish that compromise because they do not differentiate between model parameters and display parameters, although they have opposite purposes: we want many display parameters for an accurate representation but, at the same time, few model parameters for an inexpensive inversion. (An example of this will be explained below.) If we decide to use any other basis function instead of square pixels, we always have to discretize it fine enough to ensure

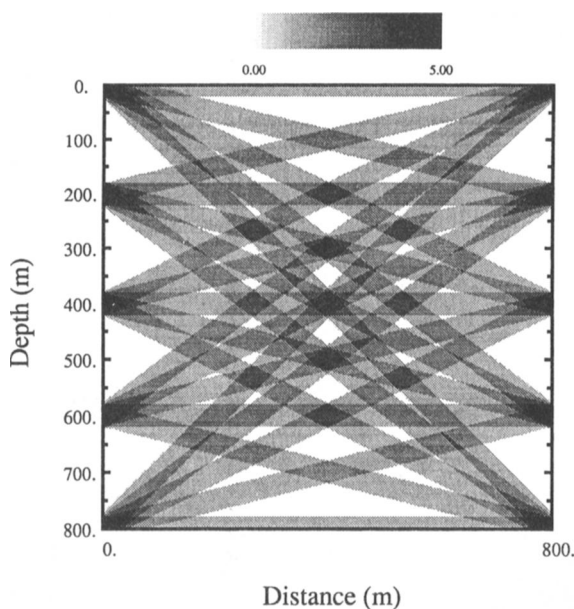


FIG. 3. Natural pixels in a constant slowness medium for a crosswell configuration of five sources and five receivers.

the numerical accuracy in the summation (21), but this fact does not change the number of model parameters.

The coefficients  $a_n$  in equation (21) represent all the information gained from the measurements, which can be seen easily when only one measurement is available. In this case, the coefficient  $a_1$  is proportional to the average slowness in the region of the beam path. If we want to invert that measurement using square pixels, the problem in general will be underdetermined or, in the best case (using only one pixel in the inversion), we can obtain information not present in the data, e.g., information outside the spatial support of the observation.

Each travelttime measurement *does not* contain information about variations in the slowness along the beampath. The variations are averaged into a single number, the travelttime, and it is only the combination of them overlapping beampaths that gives information about these variations. This basic fact is contradicted when the model is discretized into square pixels that potentially introduce variations along each beampath and demand from the data more information than they contain. Introducing more degrees of freedom into the problem might be convenient if there is enough information to resolve all of them. The extra information needed to solve the problem is introduced in the form of constraints, some of them resulting from independent data and others are simply "reasonable" constraints. Smoothness is an example of a reasonable constraint that helps solve the problem of the extra information needed. However, it is not clear how the solution may depend upon the various ways of introducing the smoothness (Claerbout, 1976) or other reasonable constraints that do not come from independent observations.

To this point, the inversion is strictly linear, which means that the sampling functions do not depend upon the slowness. This is analogous to Fourier reconstruction where the sampling functions (complex exponentials) do not depend upon the properties of the unknown. No iterations are needed after the estimate is found. The situation is different in travelttime tomography where the sampling functions may strongly depend upon the unknown slowness (the next section addresses this topic).

### Iterative inversion

The travelttime along a ray in a medium of slowness  $S(x, y)$  is

$$t = \int_{\ell} S(x, y) d\ell, \quad (26)$$

where the travelttimes as well as the raypaths depend upon the slowness. When the raypaths are straight lines, like in X-ray tomography, or when the variations in slowness are small, we can derive  $S(x, y)$  from the travelttimes using this expression. In geophysical applications, however, straight rays are rarely found, and as a result, the inversion problem (26) becomes highly nonlinear since the unknown  $S(x, y)$  is also implicitly present in the raypath (Nolet, 1987).

If the medium is perturbed to  $S'(x, y) = S(x, y) + \Delta S(x, y)$ , the new travelttime calculated along the new raypath  $\ell'$  is

$$t' = \int_{\ell'} S'(x, y) d\ell'. \quad (27)$$

Using Fermat's principle, it can be shown (Aki and Richards, 1980) that the difference in traveltimes between the two media is

$$\Delta t = \int_{\ell} \Delta S(x, y) d\ell, \quad (28)$$

where  $\Delta t = t' - t$ . The nonlinear problem is then solved as a sequence of linearized steps that seeks to minimize the difference between real and calculated traveltimes.

If the perturbations in traveltimes are calculated as integrals along the beampaths, equation (28) becomes

$$\Delta t_m = \int_{\Omega} \Delta S(x, y) \phi_m(x, y) dx dy. \quad (29)$$

The beampaths are centered in the rays traced in the unperturbed model. Substituting  $\Delta S(x, y)$  by  $\bar{S}(x, y)$  in equation (21) and  $\Delta t_m$  by  $t_m$  in equation (22), we can get the estimate of the slowness perturbation  $\Delta S(x, y)$  after solving equation (22). This estimate reproduces the perturbations in traveltimes; thus, when the problem is linear, it converges in one iteration, like in Fourier reconstruction problems (see the examples that follow).

#### NUMERICAL EXAMPLES

We will now show synthetic inversion examples comparing natural pixels and square pixels as basis functions. Our aim is to compare the results of the inversion when both are used with the same data set. This goal can be achieved with synthetic data for a cross borehole geometry generated from the model shown in Figure 4. The example is simplified considerably by assuming that the slowness contrast between the circular disc ( $S = 2.02$ ) and the background ( $S = 2.00$ ) is 1 percent. Therefore, straight rays adequately describe the propagation of the energy in the medium.

The data are generated from strip integrals across the model of Figure 4. The integrals are calculated from the analytical expressions of the intersection of the strips with the circle. In this way the numerical errors in the forward modeled data have been minimized. Two-hundred eighty-nine traveltimes were computed, which corresponds to the 17 sources and 17 receivers used. Another simplification is made assuming that the width of the strips  $\lambda' = 40$  m is the same during both the forward modeling and the inversion.

When the model is discretized into square pixels, the estimate of  $\Delta S(x, y)$  [equation (29)] is obtained after solving a system of linear equations where the matrix coefficients represent the area of the intersection of the strip with each pixel. We solved this system and the one obtained with the natural pixels [equation (22)] using the LSQR variant of the conjugate gradient method (Nolet, 1987) that has been proven to be faster than SIRT methods (Nolet, 1985; Van der Sluis and Van der Vorst, 1987).

Figures 5 and 6 show the results of the inversion when the model is discretized with two different pixel sizes. The starting model has a constant slowness  $S_0(x, y) = 2$ . The

inversion produces directly the slowness value in each pixel, and therefore, reducing the size of the pixels (for better resolution) increases the number of model parameters and consequently the size of the system of equations to solve. In the examples shown, the size of the system of equations solved is  $289 \times 1681$  (grid size =  $41 \times 41$ ; Figure 5) and  $289 \times 25921$  (grid size =  $161 \times 161$ ; Figure 6), respectively.

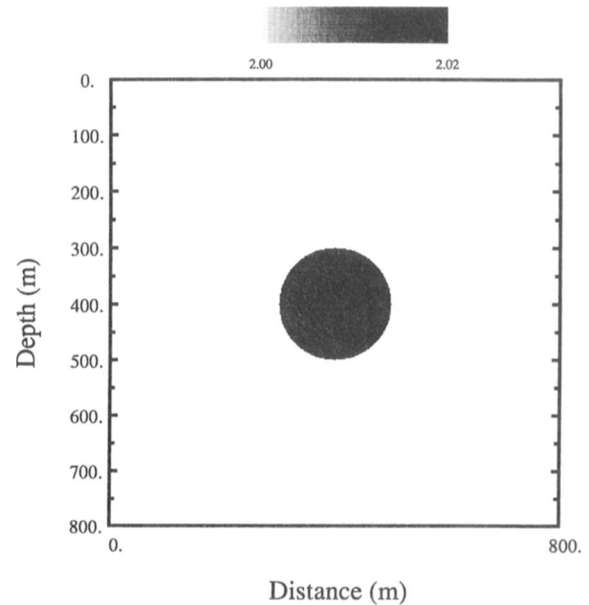


FIG. 4. Slowness perturbation. 17 sources are located on the right-hand side of the model and 17 receivers are located on the opposite side. The radius of the disc is  $r = 100$  m. The width of the natural pixels is  $\lambda' = 40$  m. The vertical separation between adjacent sources and/or receivers is 50 m.

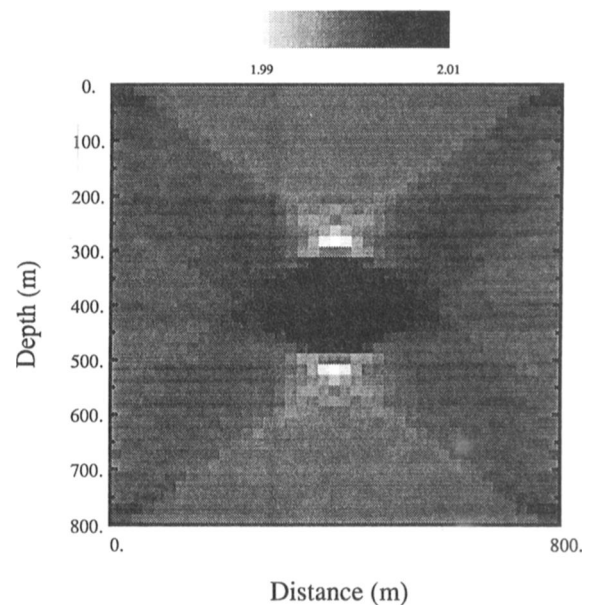


FIG. 5. Inversion when a grid of  $41 \times 41$  square pixels is used.

Evidently, the quality of the reconstruction and the amount of information about the model contained in the image increases with the number of model parameters. Note that no interpolating or smoothing process has been applied to the images. The coarse discretization and the limited view of the data are the causes of the artifacts in Figure 5.

The result of the inversion using natural pixels is shown in Figure 7 (see the Appendix for details in the implementation). This image is represented with a grid identical to the one used in Figure 6 ( $161 \times 161$ ) and then both results can be

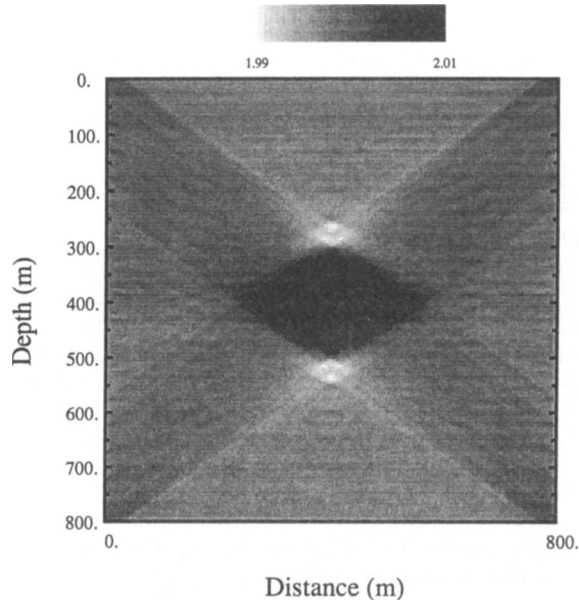


FIG. 6. Inversion when a grid of  $161 \times 161$  square pixels is used.

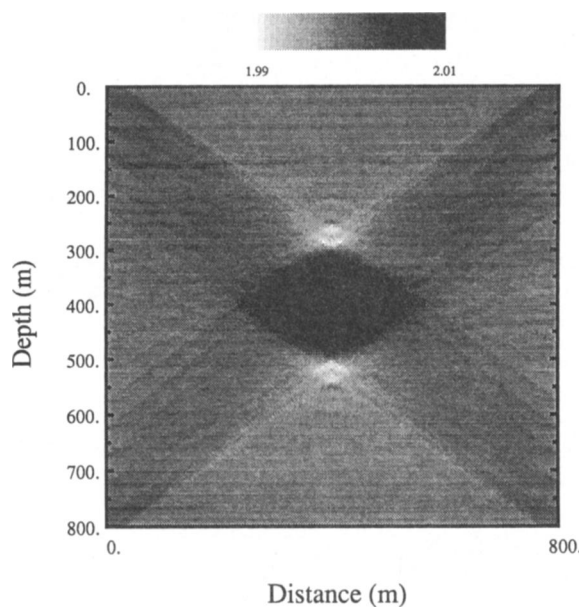


FIG. 7. Inversion when the model is discretized in natural pixels. The image is displayed in a grid of  $161 \times 161$  cells.

compared directly. The system of equations solved with the natural pixels is  $289 \times 289$ , and these dimensions are independent of the level of resolution of the image.

The images look almost identical in terms of resolution. The artifacts produced by a coarse sampling of the model (Figure 5) have been reduced. The discretization along the natural pixels does not contribute to eliminate limited view problems in the inversion, since we can see them in both cases. The main difference between the two solutions is related with the smoothness of the image. The reconstruction with the square pixels produces a slightly smoother image than the reconstruction with the natural pixels.

For comparing the results of the inversion with square and natural pixels, we plotted the absolute value of the difference between the original image (Figure 4) and the inverted ones (Figures 6 and 7). The results are shown in Figures 8 and 9. The maximum error obtained with natural pixels is the same as obtained with square pixels. We expect both images to be roughly the same since both discretizations minimize the expression (2). This expression represents the norm of the null space of the problem  $f_2(x, y)$ . If we discretize the original image very densely (grid size =  $889 \times 889$ ), we can calculate this norm in both reconstructions. For the square pixels the result is  $\|f_2\| = 2.383$  and for the natural pixels  $\|f_2\| = 2.397$ . The norm of the null space for the inversion with less square pixels (Figure 5) is  $\|f_2\| = 2.471$ . This means that the norm of the null space is reduced by sampling the image more densely in the square-pixels-based inversion.

The noisy appearance of the inversion with natural pixel reconstruction can be reduced by sampling the strips more densely. The result is shown in Figure 10, where a grid of  $401 \times 401$  points has been used. The norm of the null space of this image is  $\|f_2\| = 2.394$ . The extra computations necessary for producing the image from the digitized beampaths [equa-

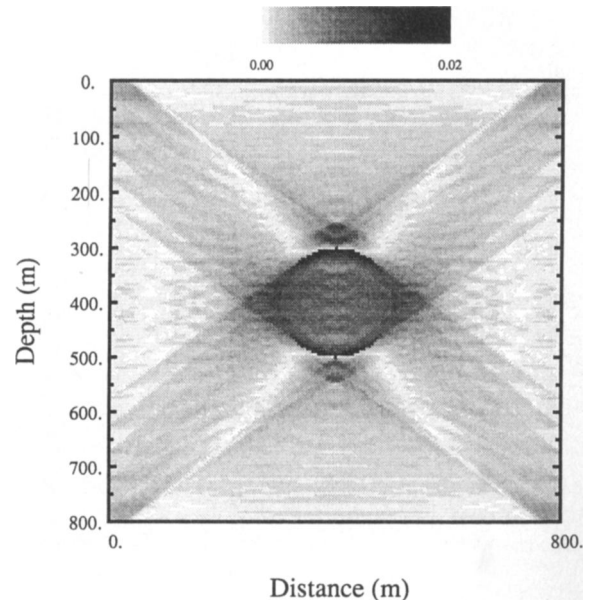


FIG. 8. Error in the inversion with square pixels. This image represents the absolute value of the difference between the original model (Figure 4) and the inverted one (Figure 6).

tion (21)] are negligible compared with the computation of the matrix elements and the solution of the system of equations for the coefficients of the square pixels. Once the coefficients  $a_n$  for the natural pixels are obtained, the image can be displayed using different grid sizes without having to build a new matrix and solve the system of equations again.

We can also compare the mean absolute error in both images from the following expression:

$$\text{error} = \frac{1}{N} \sum_{i=1}^N |(\text{original pixel})_i - (\text{reconstructed pixel})_i|, \quad (30)$$

where  $N$  in this case represents the total number of cells.

For the natural pixels as well as for the square pixels, the mean error is  $2.0 \cdot 10^{-3}$ . However, remember that although the quality of the inversion is basically the same for both basis functions, the computational effort necessary in the whole process is roughly two orders of magnitude smaller when natural pixels are used and both images are densely sampled with the same number of points.

The sizes of the matrices involved in the previous inversions are  $289 \times 1681$  and  $289 \times 25921$  for the square pixels and  $289 \times 289$  for the natural pixels. The first and the last matrices allow the computation of the singular values in a reasonable time. The results are shown in Figure 11, where the curve labeled 3 (upper curve) refers to the natural pixels discretization and the curve 1 to the  $289 \times 1681$  matrix obtained when square pixels are used. Curve 2 represents the singular values of the matrix obtained when the model is discretized in a grid of  $17 \times 17$  square pixels (size of the matrix  $289 \times 289$ , the same as the matrix in curve 3). The matrix computed as intersections of natural pixels (curve 3) is significantly better conditioned than the other two matrices. Sampling the image more densely also makes the square pixel matrices (curves 1 and 2) better conditioned.

## CONCLUSIONS

We have shown that the natural pixels provide an efficient way of discretizing the slowness model in the problem of traveltime tomographic inversion. In the examples studied, images of similar quality were obtained using natural pixels compared with the traditional reconstruction of square pixels. The main advantage of the natural pixels is that the number of model parameters needed is two orders of magnitude smaller, which means a proportional reduction on the

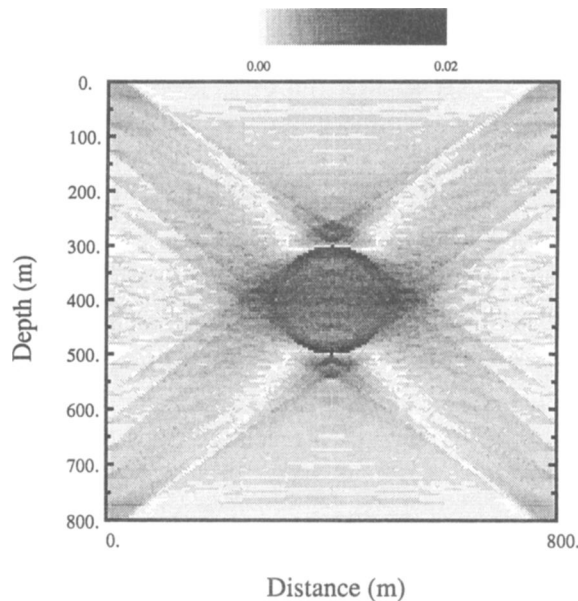


FIG. 9. Error in the inversion using natural pixels. This image represents the absolute value of the difference between the original model (Figure 4) and the inverted one (Figure 7).

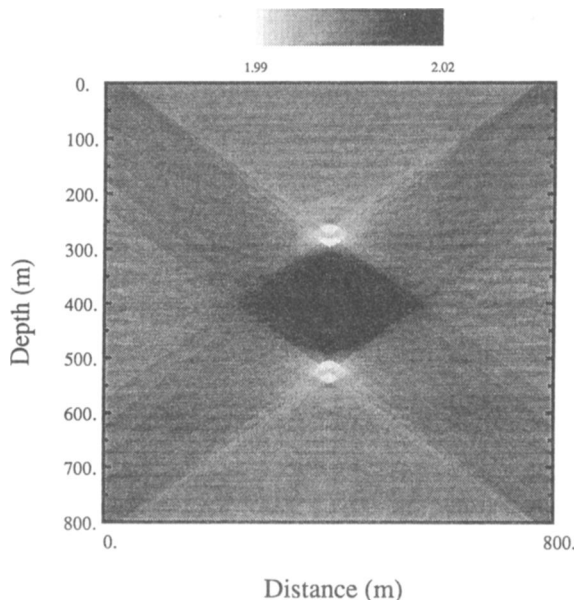


FIG. 10. Inversion when the model is discretized in natural pixels. The image is displayed in a grid of  $401 \times 401$  cells.

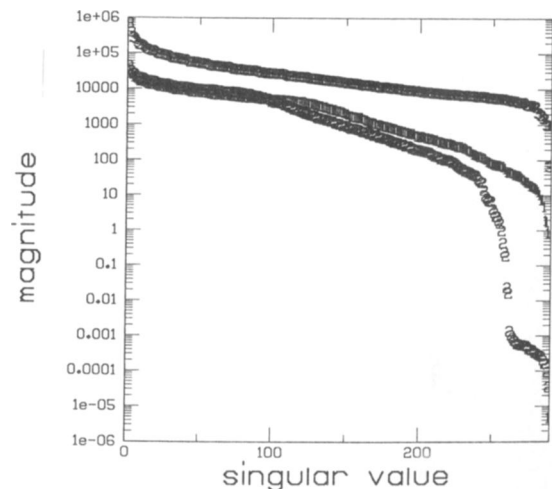


FIG. 11. Singular value decomposition for the matrices obtained with different discretizations: (1)  $41 \times 41$  square pixels, (2)  $17 \times 17$  square pixels, and (3) natural pixels.



computational effort. Besides that, the inversion with the natural pixels is better conditioned than the inversion with square pixels when comparable numbers of parameters are used.

To obtain the estimate  $\bar{S}(x, y)$  with natural pixels, two different minimization problems are involved. The first one is implied by equation (9), where the function to be minimized is the error between the true *model* and the estimated one. The second minimization problem is related to the solution of the system of equations (22), where the function to be minimized is the error between observed and calculated *data*. We have shown the importance of the first minimization in terms of the computational effort required to obtain the final estimate.

The number of natural pixels equals the number of data points, which means that the number of model parameters in the inversion remains *constant* for a fixed amount of data, regardless of the spatial dimensions of the problem or the resolution of the display. Consequently, the natural pixels provide a direct procedure for inversion in three dimensions, problems that can be computationally impossible to attack if the model is described with orthogonal 3-D pixels (boxes).

The discretization of the model along the natural pixels will change in general from one experiment to another and from one iteration to another within the same inversion, since the natural pixels may change in each of these situations. In this sense, we can say that the discretization is flexible because it depends upon the given data. However, some flexibility is lost if we want to introduce information not described by natural pixels such as known boundaries or slowness in some areas.

More research has to be done to determine the most appropriate function that approximates the beampaths (instead of the natural pixels described herein), depending upon the characteristics of the data set. Woodward (1989) gives important indications about this problem describing the beampaths (wavepaths) as elliptical, multiple-Fresnel-zone patterns, analogous to the migration ellipses. The width of her wavepaths is inversely proportional to the bandwidth and it is independent on the central frequency. Woodward's wavepaths are calculated using finite differences, which

might not be convenient when large data sets are inverted with our method of discretization.

#### ACKNOWLEDGMENTS

We would like to thank Spyros Lazaratos for many interesting discussions and important suggestions. The first author thanks INTEVEP, S.A. for financial support. The reviewers' comments and suggestions are also gratefully acknowledged.

#### REFERENCES

- Aki, K., and Richards, P. G., 1980. Quantitative seismology: W. H. Freeman and Co.
- Berberian, S. K., 1976. Introduction to Hilbert space: Chelsea Publ. Co.
- Buonocore, M. H., 1981. Fast minimum variance estimator for limited angle computed tomography image reconstruction: Ph.D. thesis, Stanford Univ.
- Buonocore, M. H., Brody, W. R., and Macosvski, A., 1981. A natural pixel decomposition for two dimensional image reconstruction: IEEE Trans. Biomedical Engineering, **BME-28**, 69-78.
- Claerbout, J. F., 1976. Fundamentals of geophysical data processing: McGraw-Hill Book Co.
- Darling, A. M., Hall, T. J., and Fiddy, M. A., 1983. Stable noniterative object reconstruction from incomplete data using a priori knowledge: J. Opt. Soc. Am., **73**, 1466-1469.
- Harlan, W. S., 1989. Tomographic estimation of seismic velocities from reflected raypaths: Presented at the 59th Ann. Internat. Mtg., Soc. Expl. Geophys., Expanded Abstracts, 922-924.
- Ivansson, S., 1985. A study of methods for tomographic velocity estimation in the presence of low velocity zones: Geophysics, **50**, 969-988.
- McMechan, G. A., 1983. Seismic tomography in boreholes: Geophys. J. Roy. Astr. Soc., **74**, 601-612.
- Nolet, G., 1985. Solving or resolving inadequate and noisy tomographic systems: J. Comp. Phys. **61**, 463-482.
- 1987. Seismic wave propagation and seismic tomography, in Nolet, G., Ed., Seismic tomography: D. Reidel Publ. Co., 1-23.
- Stakgold, I., 1979. Green's functions and boundary value problems: John Wiley & Sons, Inc.
- Van der Sluis, A., and Van der Vorst, H. A., 1987. Numerical solution of large, sparse linear algebraic systems arising from tomography problems, in Nolet, G., Ed., Seismic tomography: D. Reidel Publ. Co., 49-84.
- Van Trier, J., 1988. Migration velocity analysis using geological constraints: Presented at the 58th Ann. Internat. Mtg., Soc. Expl. Geophys., Expanded Abstracts, 897-900.
- Woodward, M. J., 1989. Wave equation tomography: Ph.D. thesis, Stanford Univ.

#### APPENDIX

##### IMPLEMENTATION OF THE INVERSION USING NATURAL PIXELS (IN TWO DIMENSIONS)

The step-by-step computational procedure for iterative traveltime inversion using natural pixels is summarized in this appendix.

**Step 1:** Calculate the synthetic traveltimes in the given (initial) slowness model using equation (20) and the definition of natural pixels. This equation is a surface integral (in 2-D). Surface integrals are difficult to evaluate especially if there is no analytical expression for the integrand. However, once a ray has been traced (Figure A-1), this integral can be evaluated simply and accurately with the expression

$$t_m = \frac{1}{\lambda'} \sum_{i=1}^{N_{x_m}} S_i \Delta \ell_{m_i} \lambda' = \sum_{i=1}^{N_{x_m}} S_i \Delta \ell_{m_i} \quad (\text{A-1})$$

Strictly speaking,  $S_i$  is the average slowness in the *subarea*  $\Delta \ell_{m_i} \lambda'$  of the natural pixel  $m$  of width  $\lambda'$  and ray segment

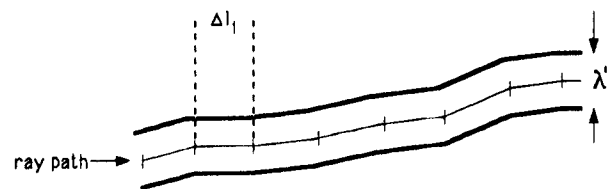


FIG. A-1. Detail of a natural pixel. The traveltime along a natural pixel is equal to the sum of products  $\Delta l_i \times (\text{slowness})_i$ , where  $(\text{slowness})_i$  can be approximated by the average slowness perpendicular to the ray segment.

length  $\Delta\ell_m$ . However,  $S_i$  can be approximated by the average slowness across the natural pixel at any position along the ray segment.  $N_{x_m}$  is the total number of segments for the  $m$ th ray.

It is clear that when the model is homogeneous, the traveltimes calculated in this fashion are equal to those calculated conventionally as line integrals across the model. Differences arise when the model is heterogeneous, because the traveltimes calculated with the natural pixels also "see" the neighborhood of the ray.

**Step 2:** Compute the traveltime differences  $\Delta t_i$  of the real minus calculated traveltimes.

**Step 3:** Calculate the matrix coefficients using expression (25). Remember that the diagonal terms of the matrix represent the area of the support of each natural pixel, whereas the off diagonal terms represent the area of intersection between them. Therefore, the diagonal terms are simply

$$A_{ii} = \lambda' \ell_i, \quad (\text{A-2})$$

where  $\ell_i$  is the total length of the ray  $i$ . Although the off diagonal terms are more difficult to compute, the computation can be simplified if we assume that in the region of intersection the natural pixels can be approximated by strips, as shown in Figure A-2a. The area of intersection is

$$A_{ij} = \lambda'^2 / \sin \alpha_{ij} \quad \alpha_{ij} \neq 0; \quad (\text{A-3})$$

$\alpha_{ij}$  is the angle between rays  $i$  and  $j$  at the intersection point. This angle is zero either when  $i = j$  (diagonal terms) or when the rays  $i$  and  $j$  are locally parallel at the intersection. In these two cases the formula (A-3) is not valid. This formula is not valid either when the area of intersection lies partially outside the support of the model (for instance, in the crosshole geometry when the intersection is close to the wells, as shown in Figures A-2b and A-2c). In such situations, the area can be calculated starting from the general expression

$$\begin{aligned} A_{ij} = & (a_i - a_j)(-x_1^2 + x_2^2 + x_3^2 - x_4^2) + (b_{1i} - b_{2j})(x_2 - x_1) \\ & + (b_{1j} - b_{2i})(x_4 - x_3) + (x_3 - x_2)D_{ij} \\ & a_i > a_j, \quad b_{1i} > b_{2i}, \quad b_{1j} > b_{2j}, \end{aligned} \quad (\text{A-4})$$

where  $D_{ij} = (b_{1i} - b_{2i})$  for the situation represented in Figure A-2b and  $D_{ij} = (b_{1j} - b_{2j})$  for the situation shown in Figure A-2c. The numbers  $x_1, x_2, x_3,$  and  $x_4$  represent the horizontal coordinates of the intersection points between the different borders of the natural pixels. To use this formula to calculate, for example, the area in Figure A-2c (shaded region), it is necessary to substitute  $x_3$  and  $x_4$  (points outside the model) by  $x_{w_2}$  (boundary of the model at the intersection region). Similar kinds of substitutions can be made in other situations where the boundary of the model crosses the intersection area.

**Step 4:** Solve the system of equations

$$\begin{bmatrix} \Delta t_1 \\ \vdots \\ \Delta t_N \end{bmatrix} = \frac{1}{\lambda'^2} \begin{bmatrix} A_{11} & A_{21} & \cdots & A_{N1} \\ A_{21} & A_{22} & \cdots & A_{N2} \\ \vdots & \vdots & \ddots & \vdots \\ A_{N1} & A_{N2} & \cdots & A_{NN} \end{bmatrix} \begin{bmatrix} a_1 \\ \vdots \\ a_N \end{bmatrix}. \quad (\text{A-5})$$

This matrix is sparse and symmetric, which helps to reduce the space needed for storage and to simplify the matrix-vector multiplications if the system of equations is solved using conjugate gradients.

**Step 5:** Compute  $\Delta S$  by substituting the resultant  $a_n$  into equation (21) using the definition of natural pixels. Each natural pixel is finely discretized, the corresponding value of  $a_n/\lambda'$  is assigned to each one, and the sum of all of them is performed.

**Step 6:** For iterative inversion, update the model.

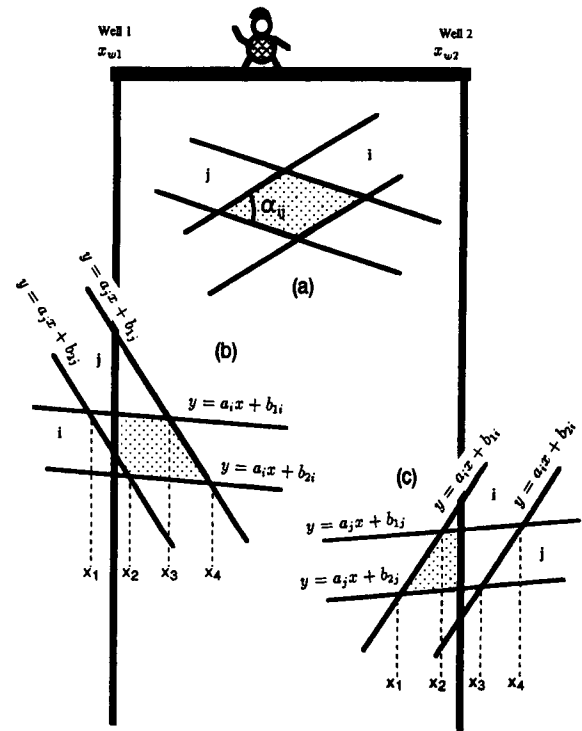


FIG. A-2. Area of intersection between two different natural pixels. (a) The intersection is completely within the model. (b) and (c) The area of intersection is partially outside the model. Note that in (b)  $x_2$  refers to the lower left corner of the parallelogram, whereas in (c)  $x_2$  refers to the upper left corner. For this reason, the formula for calculating the area varies slightly from one case to the other. In all the cases represented in this figure, the width of the natural pixels is  $\lambda'$ ;  $x_{w_1}$  and  $x_{w_2}$  are the horizontal coordinates of the wells.